ResearchGate

See discussions, stats, and author profiles for this publication at: https://www.researchgate.net/publication/268035389

Tensile deformation behavior and melting property of nano-sized ZnO particles reinforced Sn-3.0Ag-0.5Cu lead-free...

Article *in* Materials Science and Engineering A · September 2014

DOI: 10.1016/j.msea.2014.09.028

CITATIONS
7

READS
153

5 authors, including:

A. A. El-Daly
Zagazig University
45 PUBLICATIONS **785** CITATIONS
SEE PROFILE

Waled Desoky
Zagazig University
11 PUBLICATIONS **49** CITATIONS
SEE PROFILE

M. G. El-Shaarawy
Benha University
36 PUBLICATIONS **279** CITATIONS
SEE PROFILE

A. M. Abdraboh
Benha University
3 PUBLICATIONS **59** CITATIONS
SEE PROFILE

All content following this page was uploaded by Waled Desoky on 09 November 2014.

The user has requested enhancement of the downloaded file.

Materials Science & Engineering A 618 (2014) 389–397

Contents lists available at ScienceDirect

Materials Science & Engineering A

journal homepage: www.elsevier.com/locate/msea

Tensile deformation behavior and melting property of nano-sized ZnO particles reinforced Sn–3.0Ag–0.5Cu lead-free solder

A.A. El-Daly [a,*], T.A. Elmosalami [a], W.M. Desoky [a], M.G. El-Shaarawy [b], A.M. Abdraboh [b]

[a] Physics Department, Faculty of Science, Zagazig University, Zagazig, Egypt
[b] Physics Department, Faculty of Science, Banha University, Banha, Egypt

ARTICLE INFO

Article history:
Received 23 June 2014
Received in revised form
3 September 2014
Accepted 5 September 2014
Available online 16 September 2014

Keywords:
Lead-free composite solders
Microstructure
Mechanical properties

ABSTRACT

In the present study, nano-sized ZnO particle-reinforced Sn–3.0Ag–0.5Cu (SAC305) composite solder was prepared by mechanically dispersing nano-particles into SAC305 solder at 900 °C for 2 h. The effects of ZnO addition on microstructure, melting behavior and corresponding mechanical properties of SAC305 solder were explored. Microstructure analysis revealed that the wurtzite ZnO particles were effective in reducing both the β-Sn grain size and spacing between Ag_3Sn and Cu_6Sn_5 particles. The refined microstructure, which resulted in a strong adsorption effect and high surface-free energy of ZnO nanoparticles, could obstruct the dislocation slipping, and thus provides classical dispersion strengthening mechanism. This apparently enhances the yield stress (0.2%YS) and ultimate tensile strength (UTS) of SAC(305)–0.7%ZnO composite solder, whereas its ductility is lower than that of the SAC305 solder. In addition, ZnO particles keep the melting temperature of composite solder nearly at the SAC305 level although the pasty range is decreased. Empirical equations for 0.2% YS, UTS and elastic modulus *E* with the strain rate have been developed and the predicted tensile parameters for both solders are reasonably close to the present experimental data.

© 2014 Elsevier B.V. All rights reserved.

1. Introduction

With the miniaturization of modern electronic products and devices, the high packaging density of components such as chips significantly increases, and the scale of interconnections becomes smaller. Accordingly, the requirements for high integrity and reliability are challenging the solder joints performance, especially under the complicated service environments of thermal and mechanical conditions [1]. Based on these concerns, flurries of activities in electronic community have been dedicated to understanding the typical reliability issues of Pb-free solder joints [2]. Among the various lead-free solders available, Sn–Ag–Cu (SAC) series alloys have emerged as highly accepted alloys. Numerous studies have revealed that Ag content affects its thermal fatigue life and drops lifetime of soldered assembly with SAC solder joints [3]. Nevertheless, the drop performance and reliabilities of electronic assembly with SAC solder joints are worsened with increasing Ag content. Accordingly, the high Ag content SAC solders are not desirable for portable and hand-held electronic devices due to the fact that these devices have a tendency to be dropped frequently [4,5]. The formation of large intermetallic compounds (IMCs) and β-Sn dendrite deteriorates the mechanical properties of solder joints. In addition, they are more expensive due to their higher silver content. To address such demands, the low Ag content SAC alloys were considered as a solution for resolving both issues. However, reducing the Ag content of SAC alloys, such as Sn–1.0Ag–0.5Cu(SAC105), Sn–2.0Ag–0.5Cu (SAC205) and Sn–3.0Ag–0.5Cu (SAC305) alloys gives rise to more primary β-Sn phase (large β-Sn grains) and decreases the number of Ag_3Sn IMC particles [6,7]. It is therefore expected to result in lower elastic modulus and yield strength than the high Ag content SAC alloys [8]. Since the reliability of solder joints is mainly dependent on elastic modulus, mechanical strength and creep behavior, previous studies have reported that additions of nanoparticles to SAC solders could provide distinct improvement in microstructural modification and mechanical properties. These foreign dispersed second phase particles, which are induced as reinforcement, have been found to control the melt crystallization of SAC solder. In other words, reinforcing the nanoparticles can generate small sub-grain size of β-Sn phase and can offer additional obstacles to grain growth and coarsening of solder microstructure. El-Daly et al. [4,9] reported that minor addition of SiC nanoparticles significantly increased the mechanical strength of SAC105 solder and reduced the amount of undercooling during solidification, and thereby suppressed the growth of bulk Ag_3Sn plates. Shen et al. [10] added ZrO_2 nanoparticles to SAC solders and also found that ZrO_2 can reduce the undercooling and refines the Ag_3Sn IMCs. Tsao et al. [11,12] studied

* Corresponding author. University Tel.: +20 552362536; Faculty Tel.: +20 552303252; fax: +20 552308213; Mobile: +20 1271020082.
E-mail addresses: dreldaly11@yahoo.com, dreldaly@zu.edu.eg (A.A. El-Daly).

http://dx.doi.org/10.1016/j.msea.2014.09.028
0921-5093/© 2014 Elsevier B.V. All rights reserved.

the influence of reinforcing TiO_2 and Al_2O_3 nanoparticles on microstructural development and hardness of eutectic Sn–Ag–Cu solders. In their works, microhardness measurements revealed significant enhancement in the overall strength of eutectic solder. However, study on the effect of ZnO nanoparticles addition is scarce. Chuang et al. [13] and Fawzy et al. [14] investigated the effects of Al_2O_3 and ZnO nanoparticles on the microstructure, thermal property and tensile properties of Sn–3.5Ag–0.5Cu (SAC355). They reported that the liquidus temperature, 0.2% offset yield strength, and ultimate tensile strength of lead-free composite solder increase significantly with the addition of nanoparticles.

Although the effects of nanoparticles on the microstructure, thermal property and mechanical properties have been reported, the results of literature search reveal that no studies have been reported so far on SAC(305) lead-free solder containing a small amount of nano-sized ZnO particles. Accordingly, the aim of the present study is to characterize the SAC(305) solder alloys in terms of as-solidified microstructures, thermal and mechanical behavior as a function of ZnO nanoparticles content. The effect of ZnO is expected to be significant because ZnO has no solubility in β-Sn matrix. The test conditions cover the temperature and strain rate range. Processing parameters are important for the assessment of the solder joint reliability, since the solders must preserve their mechanical reliability under a myriad of conditions. The key factors that affect the mechanical behavior of the solder alloy are discussed.

2. Experimental procedures

2.1. Preparation of plain SAC(305) and composite SAC(305)–0.7%ZnO solders

Composite Sn–3.0Ag–0.5Cu solder alloy containing a small amount of ZnO nanoparticles was used in the present study. For reference, mechanical and thermal properties of plain SAC (305) alloy without ZnO nanoparticles were used. The chemical compositions of both alloys are listed in Table 1. A lead-free SAC (305) solder was prepared from bulk Sn, Ag and Cu rods (all with 4 N purity). The process of melting was carried out in a vacuum arc furnace under the protection of high purity argon atmosphere at 900 °C for about 2 h. In order to get a homogeneous composition within the ingots, the alloy was re-melted three times to produce a rod-like specimen with a diameter of about 1.5 cm. Nanocomposite SAC(305)–0.7%ZnO solder was prepared by mechanically mixing ZnO particles of about 50–100 nm into the SAC(305) alloy melt. During preparation, the pre-weighted ingot and ZnO particles were first put into an Al_2O_3 crucible and then was heated up to 450 °C. After that, an electromagnetic stirrer was activated to mechanically mix the ZnO particles into the melt for 40 min to ensure a homogeneous distribution of the reinforcing particles. Finally, it was cast with an air-cooling condition of 8.5 °C/s, so as to create a fine microstructure typically found in small solder joints in microelectronic packages.

2.2. Microstructure analysis and phase identification

The microstructure was examined by scanning electron microscopy (SEM). A solution of 2%HCl, 3%HNO_3 and 95%(vol%) Ethyl alcohol was prepared and used to etch the samples. Energy dispersive X-ray spectrometry (EDS) was adopted to identify the phase structure of the prepared sample alloys. Differential scanning calorimetry (Shimadzu DSC-50) was carried out to identify the melting process of both solder alloys. Heating and cooling the specimens in DSC analysis were carried out at 10 °C/min of heating rate in Ar flow. The solder ingots were then mechanically machined into a wire sample with a gauge length marked 4×10^{-2} m for each sample and 2.5×10^{-3} m in diameter, as developed in our previous work [9]. Before testing, the specimen was annealed at 120 °C for 45 min to reduce the residual stress induced during sample preparation. Subsequently, tensile creep tests were conducted on a 3360 universal material testing system and GWT 504 high temperature testing system, respectively. The tests were carried out at various strain rates ranging from 10^{-4} to 10^{-2} s^{-1} and constant temperature of 25 °C. Also, the tests were conducted at different temperatures ranging from 25 to 120 °C with a constant strain rate. The axial strain was measured in accordance with the ASTM: E83-10a, and ASTM D76/D76M standard practices for force verification. Then, the mechanical properties were obtained by averaging testing data. The temperature variation inside the high temperature furnace was maintained within 1.5 °C.

Table 1
Chemical composition of the solders studied (wt%).

Alloy	Cu	Ag	Fe	As	ZnO	Sb	In	Sn
SAC(305)	0.502	3.002	0.002	0.001	0.000	0.006	0.004	Bal.
SAC(305)–0.7ZnO	0.503	3.001	0.002	0.001	0.703	0.006	0.004	Bal.

3. Results and discussion

3.1. Characterization of ZnO nanoparticles

Fig. 1a and b show the bright field TEM micrographs of ZnO nanoparticles and corresponding XRD analysis of ZnO particles. Although the results confirm a slight agglomeration of ZnO particles, ZnO was uniformly distributed and appeared with slab-like particles. The slab-like particles show less polarity with a dimension of roughly 50–100 nm, which have low-aspect ratio. However, XRD analysis established the hexagonal wurtzite ZnO type structures (B4) with peak broadening, which further confirm the ZnO nano-particles. In addition, diffraction peaks corresponding to the impurity were not existent in XRD patterns, indicating the high purity of ZnO nano-powders. The characterization of morphology and uniform distribution of ZnO nano-particles inside the SAC(305)–0.7%ZnO composite solder was examined by SEM using an over-etching metallographic technique. Fig. 1c shows that ZnO nanoparticles are uniformly distributed as a bright spot inside the dark β-Sn matrix.

3.2. Microstructure of as-solidified SAC(305) and nanocomposite SAC(305)–0.7%ZnO solders

Fig. 2 shows the XRD profiles of plain SAC305 and SAC(305)–0.7%ZnO composite solders. Diffraction peaks corresponding to β-Sn, Ag_3Sn and Cu_6Sn_5 phases were mainly evidenced for both solders, as similarly reported by Fawzy et al. [14] and El-Daly et al. [15]. Due to the minor addition of ZnO nanoparticles, there are no peaks identified as ZnO in XRD spectrum. In Sn–Ag–Cu system [16], since the maximum solubility limits of Ag and Cu in Sn are 0.04 wt% and 0.0063 wt%, respectively, the peaks associated with Ag_3Sn and Cu_6Sn_5 IMCs were observed in both solders. Considering the evolution of microstructural phases for both alloys specified by SEM/EDS analysis, the microstructure of as-solidified samples with reinforcing nano-ZnO particles is shown in Fig. 3. In Fig. 3a, the solidification process of plain SAC(305) solder exhibited completely dendritic arrays of large gray β-Sn phase, which tend to be spheroids in some areas, surrounded by dark eutectic regions consisting of Ag_3Sn particles and irregular polygon Cu_6Sn_5 shapes. According to EDS analysis, the whole surface of solder matrix incorporates both the Sn, Ag and Cu elements, which

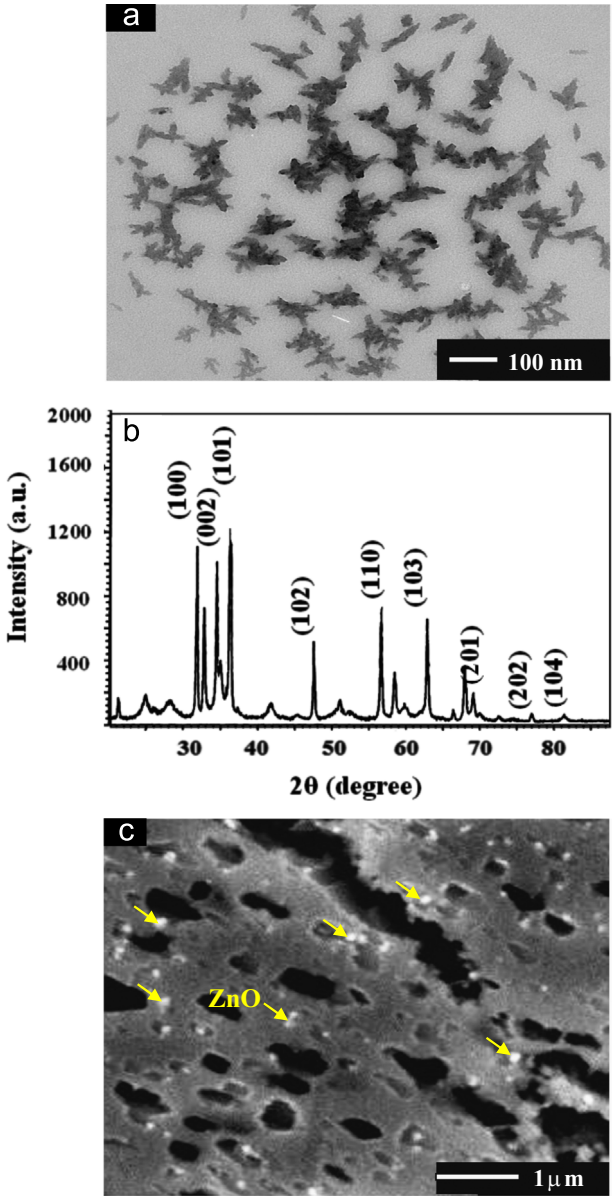

Fig. 1. (a) Bright field TEM of ZnO nanoparticles and size distribution, (b(XRD patterns of nano-sized ZnO particles, (c) Spheroids and fine dot-shaped submicron ZnO particles located on the surface of SAC(305)–0.7%ZnO solder matrix.

confirmed the presence of primary β-Sn phase, Ag_3Sn and Cu_6Sn_5 IMCs. However, the average size of β-Sn was 75 μm with an aspect ratio of 1.5. The Ag_3Sn demonstrates the coarse needle-like structures with an average particle size of 40 μm, but the size of Cu_6Sn_5 IMC is approximately 5 μm.

Grain-size refinement is a well-known strengthening structure mechanism in metals and alloys. In Fig. 3b, significant change in grain size was observed in the SAC(305)–0.7%ZnO composite solder. ZnO nanoparticles' addition to SAC305 alloy has resulted in substantial decrease of β-Sn grain size from 75 to 25 μm, which only may enhance the mechanical strength of the composite solder. The reason may be that ZnO nanoparticles promote a high nucleation density of the second phase in eutectic colony during solidification [17]. It is well known that grain refinement is a well-established process resulting in enhanced metallurgical properties such as elastic modulus, ductility, yield strength, and surface finishing characteristics. Tsao [18] also reported that the addition of nano-sized TiO_2 ceramic particles to Sn–3.5Ag–0.5Cu lead-free solder could result in microstructural refinement, uniform

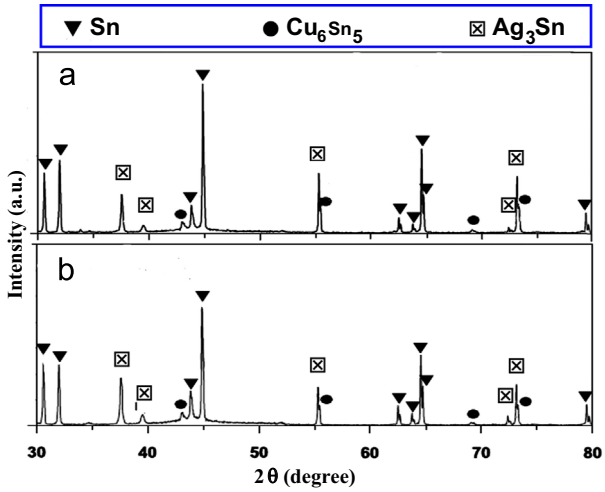

Fig. 2. XRD patterns of: (a) plain SAC (305) and (b) composite SAC(305)–0.7%ZnO solder alloys.

distribution of Ag_3Sn and Cu_6Sn_5 IMCs and small primary β-Sn grains. Recently, a similar trend was reported for microstructure results of bulk SAC(105)/SiC composite solders [4,9]. According to EDS analysis shown in Fig. 3, the whole surface of composite SAC (305)–0.7%ZnO solder matrix incorporates the Sn, Ag, Cu, Zn, and O elements, which confirmed the presence of primary β-Sn phase, Ag_3Sn and Cu_6Sn_5 IMCs as well as the ZnO particles. The decrease in β-Sn grain size of composite solder is 3 times lower than that of plain SAC305 alloy. It indicates that the ZnO nanoparticles have high ability to control grain growth during solid state cooling. In addition, reinforcing ZnO nanoparticles could improve mechanical properties and long term reliability of solders. Interestingly, the microstructure could be clear evidence of significant decrease in the needle-like Ag_3Sn particles, which are characterized by stumpy spacing. This finding is consistent with the results of SAC (355) solder alloy [14]. This type of structure can act as more effective pinning action of dislocation motion in the solder matrix, and subsequently affects its physical and mechanical properties.

3.3. *Thermal analysis of solders*

DSC is an efficient technique for quantitative thermal analysis and provides crucial information on phase transition characteristics. DSC curves recorded during heating and cooling for plain SAC305 and composite SAC(305)–0.7%ZnO solder alloys are shown in Fig. 4. The results are collected in Tables 2 and 3. During heating, the melting temperature T_m of plain SAC305 and composite SAC (305)–0.7%ZnO solders were about 220.5 °C and 220.3 °C, respectively, with only one endothermic peak. The reduction of T_m was less than 0.5 °C for SAC305 solder due to ZnO addition. The reason may be that the reinforcing nano-sized ZnO particles could modify the surface instability and physical properties of grain boundary/interfacial characteristics. Such particles may serve as restrained sites for the solidification process of IMCs as well as β-Sn grains. Wang et al. [19] also reported that the addition of a small amount of SiC particles (with an average size of 1 μm) did not significantly affect the melting point of Sn–3.7Ag–0.9Zn alloy. Moreover, these results are quite consistent with those reported for SAC(355) and SAC(103) solders [6,14].

The pasty range ($\Delta T = T_{end} - T_{onset}$) obtained in DSC calorimeter for both alloys is shown in Table 2. Here, T_{end} and T_{onset} are the measured liquidus and solidus temperatures of the solder during heating. As seen in Table 2, the pasty range occurs around 7.7 °C for SAC(305) solder. Then, ΔT was improved and dropped slightly to about 6.4 °C in composite SAC(305)–0.7%ZnO solder alloy.

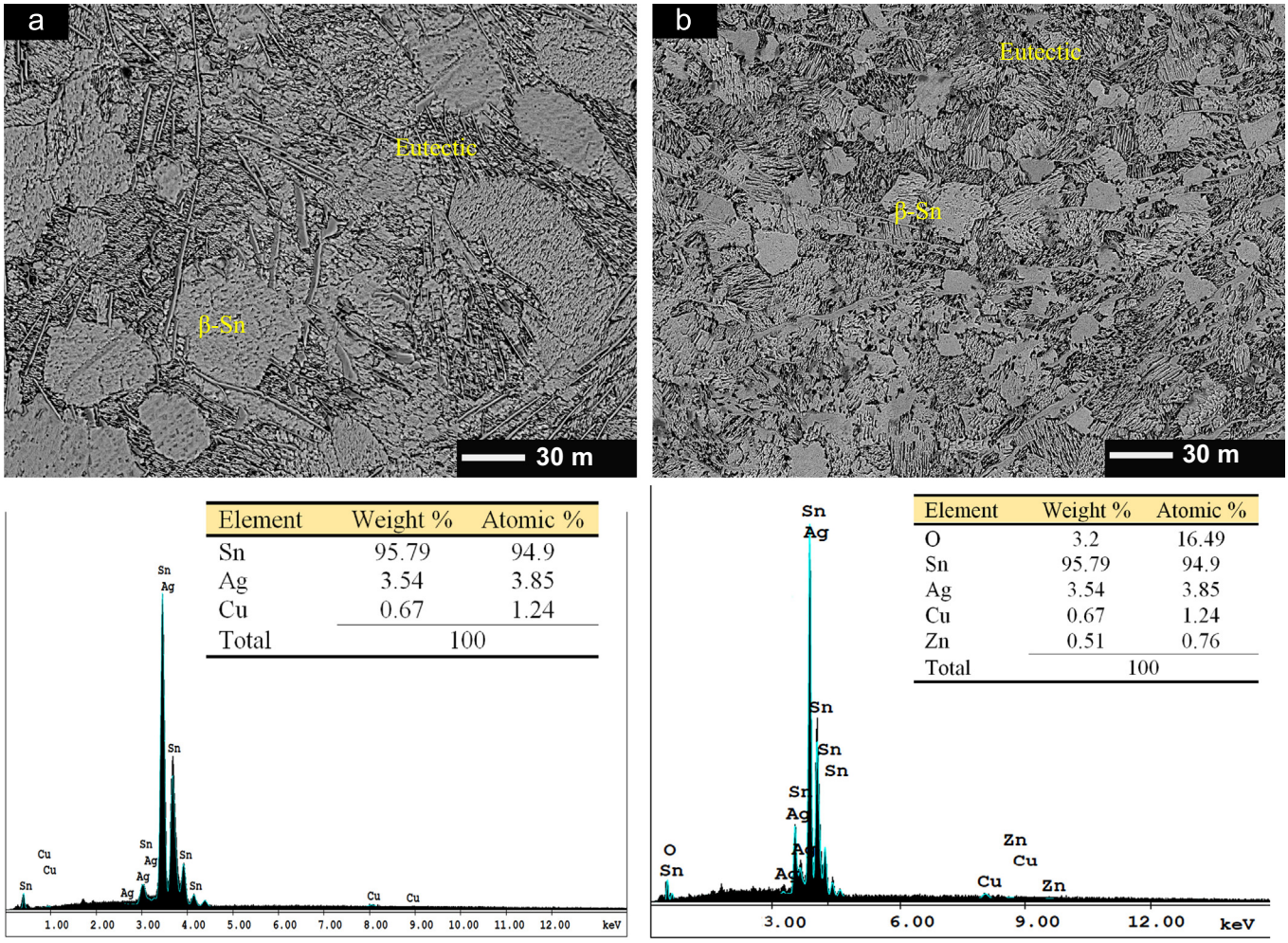

Fig. 3. SEM micrographs of: (a) SAC(305) and (b) SAC(305)–0.7%ZnO solder alloys and their corresponding EDS analysis.

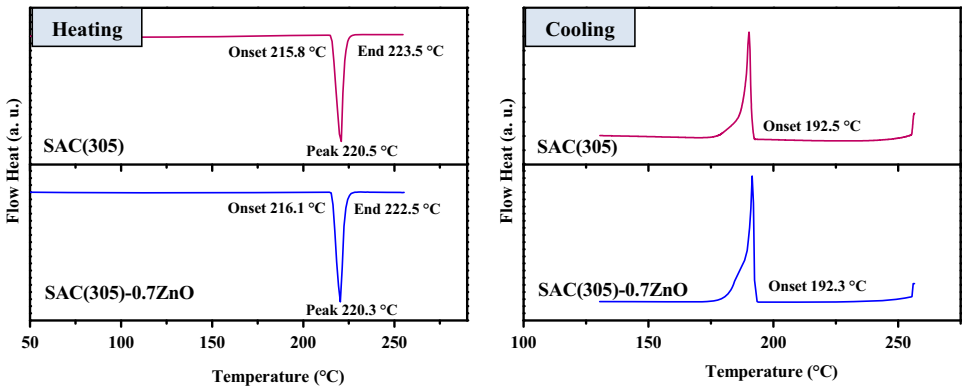

Fig. 4. DSC results during heating (endothermal) and cooling (exothermal) for SAC(305) and SAC(305)–0.7%ZnO solders.

Table 2
Solidus temperature (T_{onset}), liquidus temperature (T_{end}), Pasty range and melting temperature for SAC(305) and SAC(305)–0.7ZnO solder alloys from heating curve.

Alloy	(T_{onset}) (°C)	T_{end} (°C)	Pasty range ($T_{end} - T_{onset}$) (°C)	Melting temperature (°C)
SAC(305)	215.8	223.5	7.7	220.5
SAC(305)–0.7ZnO	216.1	222.5	6.4	220.3

Table 3
Undercooling range for SAC(305) and SAC(305)–0.7ZnO solder alloys.

Alloy	(T_{onset}) heating (°C)	T_{onset} cooling (°C)	Undercooling (°C)
SAC(305)	215.8	192.5	23.3
SAC(305)–0.7ZnO	216.1	192.3	23.8

In comparison with the pasty range of 11.5 °C for Sn–Pb solder alloys [6], the present solders have the lowest one. Apparently, the small pasty range is likely to alleviate some manufacturing problems, such as increasing the probability of fillet lifting phenomena and the tendency towards porosity and hot tearing contraction during solidification [20].

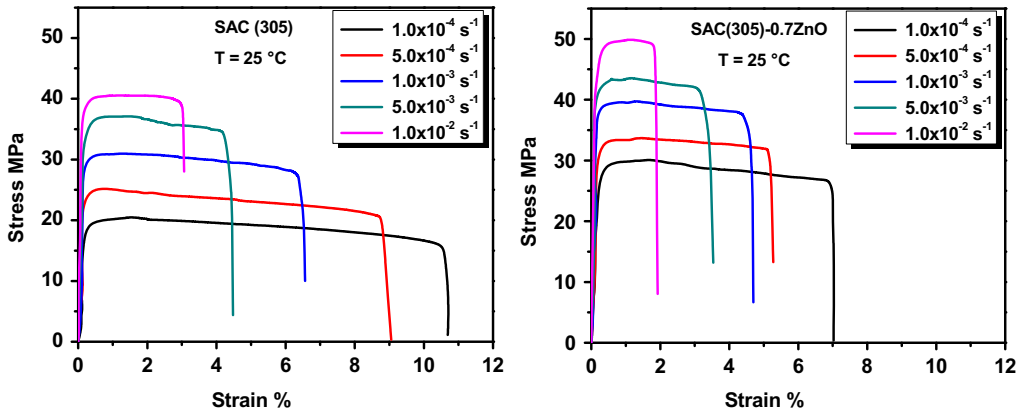

Fig. 5. Tensile properties of SAC(305) and SAC(305)–0.7%ZnO solder alloys at constant temperature and different strain rates.

Table 4
Tensile properties of SAC (305) and SAC(305)–0.7ZnO solder alloys at room temperature and strain rate of $1 \times 10^{-3}\ s^{-1}$.

Alloy	Elastic modulus (GPa)	UTS (MPa)	0.2%YS (MPa)	Elongation (%)
SAC(305)	36.24	30.94	28.99	6.5
SAC(305)–0.7ZnO	52.36	39.85	37.02	4.7

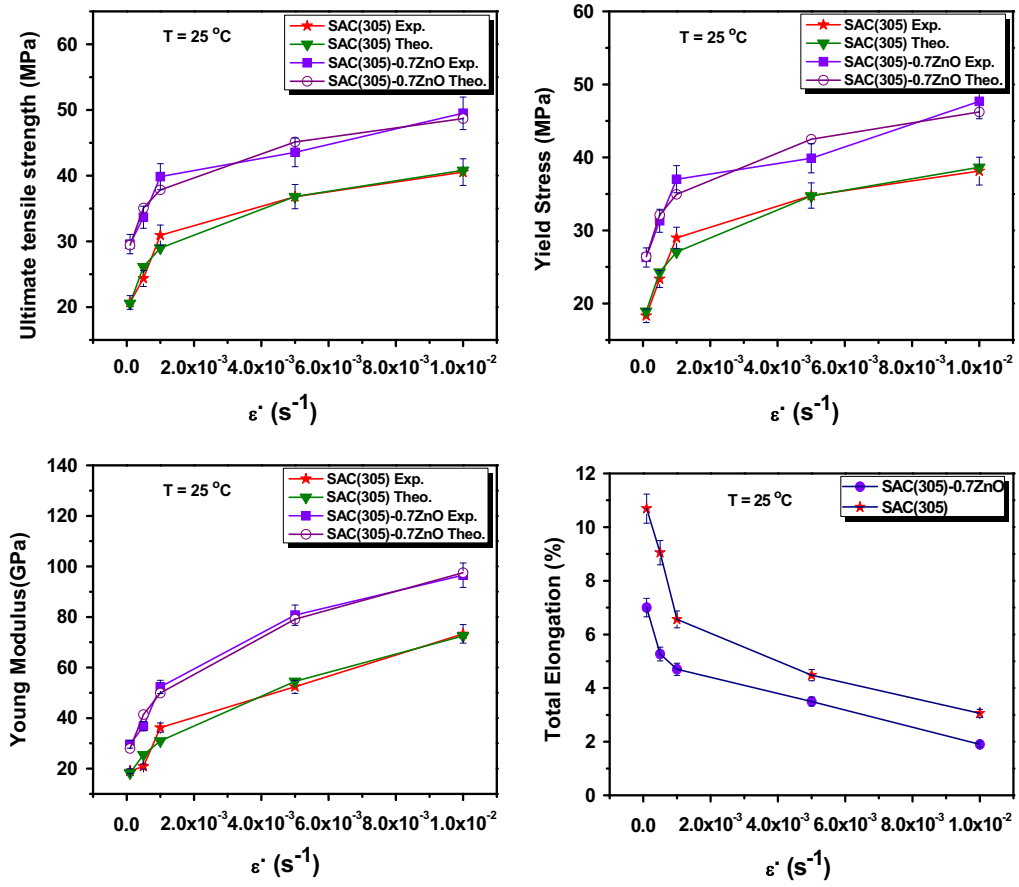

Fig.6. Experimental and theoretical mechanical property data for SAC(305) and SAC(305)–0.7%ZnO solder alloys at various strain rates.

Undercooling is defined as the difference between the T_{onset} during heating and T_{onset} associated with cooling, and relates to the difficulty of nucleating the solid phase in a liquid state [21]. Due to undercooling, the exothermal peaks upon cooling for both alloys emerged at lower temperatures compared with their endothermal peaks, but the reductions in temperature were not the same as seen in Fig. 4 and Table 3. Notably, the degree of undercooling for SAC (305) solder was slightly increased from 23.3 to 23.8 °C with ZnO nanoparticles' addition. These results propose that the undercooling achieved in the DSC analysis is strongly dependent on the primarily nucleating β-Sn solid phase. In the composite SAC(305)–0.7%ZnO solder, as the undercooling

increases, the primary β-Sn phase transforms from coarse dendrites to refined grains of dendritic fragments.

3.4. Mechanical properties

3.4.1. Effect of strain rate on the mechanical properties of solders

Flow stress–strain curves of plain and developed SAC(305) composite solders at room temperature and different strain rates are shown in Fig. 5. The presence of ZnO nanoparticles in SAC (305)–0.7%ZnO composite solder was found to enhance significantly the tensile behavior at different strain rates. It is seen that the elastic modulus E, UTS and YS of SAC(305)–0.7%ZnO are increased while the ductility is decreased. The plausible explanation for the enhancement of mechanical properties may be due to the increase in dislocation density at the interface of ZnO nanoparticles/solder matrix and its effect on retarding the growth of overall IMC and β-Sn phase, as well as the minimal agglomeration of ZnO particles during melting of solders. For example, at strain rate of $1 \times 10^{-3}\ s^{-1}$, the elastic modulus E, UTS and YS increased from 36.24 GPa, 30.94 MPa and 28.99 MPa to 52.36 GPa, 39.85 MPa and 37.02 MPa with the addition of ZnO, respectively (Table 4). In view of the fact that the small amount of ZnO nanoparticles could act as an obstacle for dislocation motion, it is concluded that the addition of ZnO nanoparticles to SAC(305) alloy results in an excellent combination of high strength and elastic modulus in comparison with SAC(305) alloy. According to Orowan theory, the mechanical strength of solder matrix is inversely proportional to inter-particle distance, which corresponds to a dispersion strengthening mechanism.

Although the individual tensile curves shown in Fig. 5 do not always display a pronounced plateau flow at all strain rates investigated, they all eventually show a slight flow softening at lower strain rates. The possibility was that the softening beyond a given strain occurred as a result of the recovery process due to the annihilation of point defects and line defects, since there is more sufficient time for the motion of dislocations. However, the overall level of stress–strain curves is raised as the strain rate increases. Fig. 6 shows the effect of strain rate on the values of *E*, UTS, YS and total elongations for two alloys obtained at room temperature. Both alloys demonstrated an increase in *E*, UTS and YS with increasing strain rate while the elongation was decreased, indicating that the tensile behavior of the three alloys is strain rate-dependent. The SAC(305)–0.7%ZnO composite solder exhibits larger E, UTS, YS compared with the plain SAC(305) solder. Based on the experimental results, it is assumed that the mechanical properties including the *E*, YS and UTS are related to the strain rate by the following empirical relations:

$$E(\dot{\varepsilon}) = a_1\ (\dot{\varepsilon})^{a_2} + a_3 \tag{1}$$

$$\mathrm{YS}(\dot{\varepsilon}) = b_1(\dot{\varepsilon})^{b_2} \tag{2}$$

$$\mathrm{UTS}(\dot{\varepsilon}) = c_1\ (\dot{\varepsilon})^{c_2} \tag{3}$$

where a_1, a_2, a_3, b_1, b_2, c_1 and c_2 are material constants, which are obtained from the nonlinear regression and are listed in Table 5 for both solder compositions. The calculated values of mechanical properties compared with experimental results are shown in Fig.6

Table 5
Material constants in the rate-dependent mechanical property models of (1)–(3).

Solders	a_1 (GPa)	a_2	a_3 (GPa)	b_1 (MPa)	b_2	c_1 (MPa)	c_2
SAC(305)	647.3	0.5176	12.83	78.93	0.155	80.97	0.1487
SAC(305)–0.7ZnO	416.01	0.3366	9.229	80.89	0.1215	80.54	0.1093

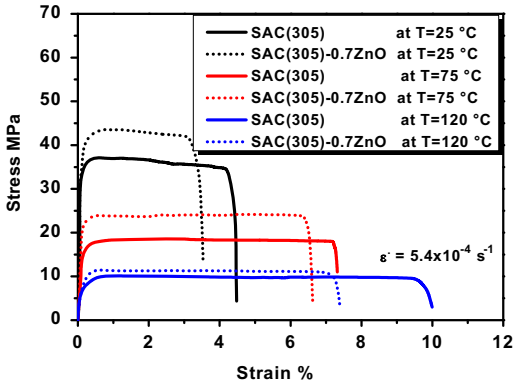

Fig. 7. Tensile properties of SAC(305) and SAC(305)–0.7%ZnO solder alloys at constant strain rate and different temperatures.

Table 6
Experimental and theoretical mechanical property data for different solders at various strain rates.

Solders/strain rate (s^{-1})	Experimental values			Theoretical values		
	E (GPa)	Yield (MPa)	UTS (MPa)	*E* (GPa)	Yield (MPa)	UTS (MPa)
SAC (305)						
1.0E−5	–	–	–	14.50	13.25	14.62
5.0E−5	–	–	–	16.67	17.01	18.57
1.0E−4	19.02	18.31	20.7	18.33	18.93	20.58
5.0E−4	20.85	23.35	24.36	25.49	24.29	26.15
1.0E−3	36.24	28.99	30.94	30.95	27.05	28.99
5.0E−3	52.38	34.78	36.81	54.52	34.72	36.82
1.0E−2	73.33	38.13	40.55	72.52	38.66	40.82
5.0E−2	–	–	–	150.13	49.61	51.86
1.0E−1	–	–	–	209.39	55.24	57.49
SAC (305)–0.7ZnO						
1.0E−5	–	–	–	17.86	19.97	22.88
5.0E−5	–	–	–	24.06	24.28	27.28
1.0E−4	29.62	26.31	29.59	27.96	26.41	29.43
5.0E−4	36.81	31.33	33.68	41.43	32.12	35.09
1.0E−3	52.36	37.02	39.85	49.90	34.94	37.85
5.0E-3	80.73	39.88	43.55	79.14	42.49	45.13
1.0E−2	96.52	47.68	49.50	97.51	46.22	48.68
5.0E−2	–	–	–	160.99	56.21	58.05
1.0E−1	–	–	–	200.87	61.14	62.61

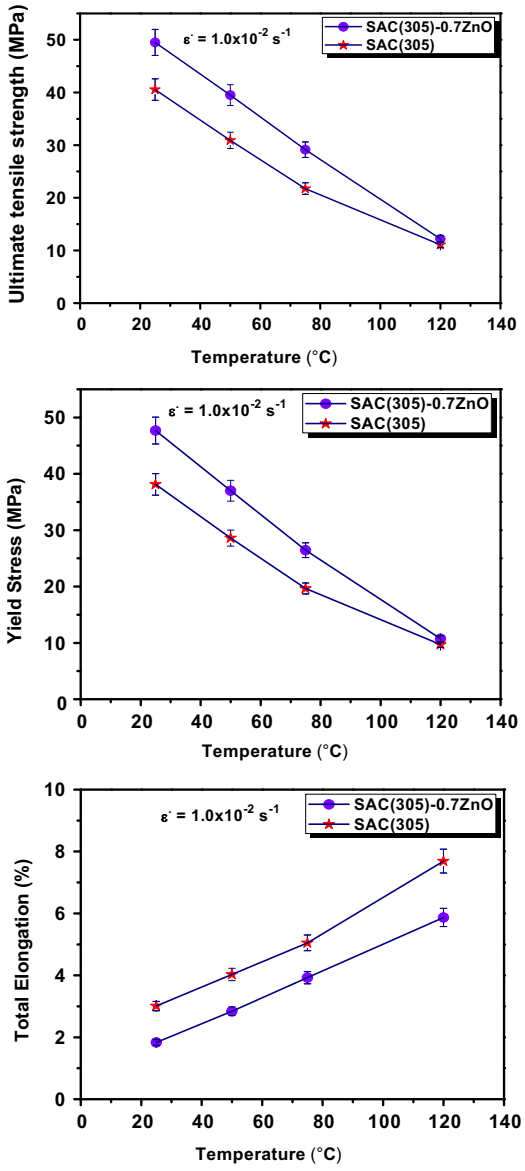

Fig.8. Effect of temperature on: ultimate tensile strength (UTS), yield stress (0.2% YS) and elongation (El. %) at strain rate of $1.0\times10^{-2}\,s^{-1}$ for SAC(305) and SAC (305)–0.7%ZnO solder alloys.

and are listed in Table 6. It is seen that the theoretical models are accurate with the errors within 1.1–12.3% for the predicted elastic modulus, 0.8–7.4% for the predicted yield stress and 0.2–6.6% for the predicted UTS.

3.4.2. *Effect of temperature on the mechanical properties*

The effect of testing temperature on tensile properties of both solders at a strain rate of $5.4\times10^{-4}\,s^{-1}$ is shown in Fig. 7. The results of ambient temperature tensile tests are shown in Fig. 8. For two alloys, it can be seen that the UTS and 0.2% YS decrease with increasing temperature, while the ductility as measured by percent elongation has increased. Similar results were obtained in our earlier studies on SAC105 and SAC305 solders [6,7]. It is to be noted that the room-temperature strengthening effect of ZnO is not persistent at high temperatures. Basically, the higher softening in both solders suggests that the interface between the small particles and solder matrix is also affected at higher temperatures. In such a case, the rate of diminish in dislocation density (annihilation) increases and promotes the continuous falling of stress level in both solders. But, the ZnO nanoparticles can act as barriers for dislocation motion and slow down the diffusion process required for proper recovery. However, significant improvement in 0.2% YS and UTS of SAC(305) solder with the addition of 0.7% ZnO nanoparticles is observed, but the ductility was lowered at all temperature ranges investigated. The high strength level of SAC(305)–0.7%ZnO composite solder can primarily be attributed to grain refinement and load transfer to the reasonably distributed harder ZnO particulate/intermetallic phases (Fig.3).

3.5. *Kinetic analysis of SAC(305)-based solders during hot deformation*

It is generally accepted that tensile strain rate of a metallic material can be correlated with the applied stress by the well-known Dorn power law equation [6]:

$$\dot{\varepsilon} = A\sigma^{n}\exp(-Q/RT) \tag{4}$$

where A is a constant; R is the universal gas constant; n is the stress exponent constant related to strain rate $\dot{\varepsilon}$; T (K) is thermodynamic deformation temperature; σ (MPa) means peak stress or UTS; and Q (kJ/mol) is the activation energy of deformation. According to Eq. (4), the slope of each line in Fig. 9 gives the stress exponent n. The values of n are listed in Table 7. It can be seen at room temperature that the n-value of plain solder

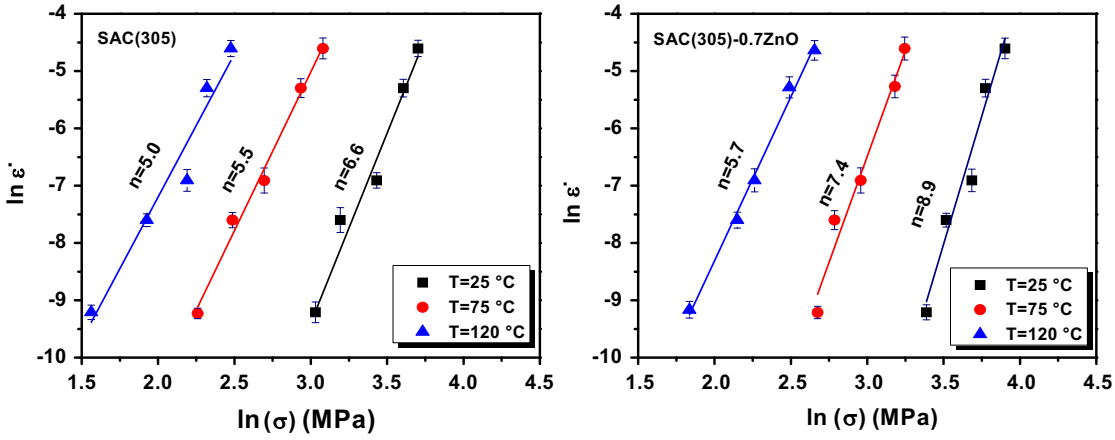

Fig. 9. Relationship between ln (σ) and ln ($\dot{\varepsilon}$) for calculation n values at different temperatures for SAC(305) and SAC(305)–0.7%ZnO solder alloys.

Table 7
Activation energy (Q) and stress exponent (n) values for SAC(305) and SAC(305)–0.7ZnO solder alloys.

Alloy	Q (kJ/mol)	Temperature (°C)	n
SAC(305)	65.6	25	6.5
		70	5.5
		120	5.0
SAC(305)–0.7ZnO	103.7	25	8.9
		70	7.4
		120	5.7

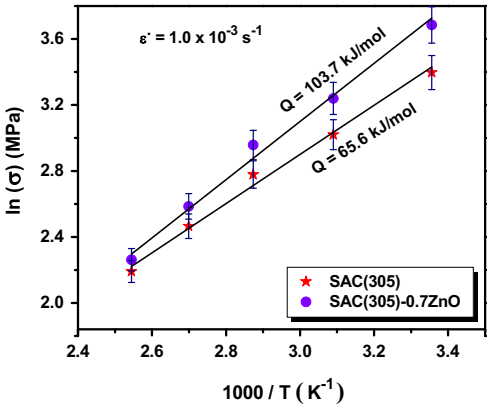

Fig. 10. The activation energy (Q) values of SAC(305) and SAC(305)–0.7%ZnO solder alloys.

increased from 6.6 to 8.9 with ZnO addition. Fig. 9 also reveals that the temperature can obviously influence the level of mechanical strength of plain and composite solder materials, and the n-value evidently deteriorates at elevated test temperatures. Moreover, the n-values decrease from 6.6 and 8.9 at 25 °C to 5.0 and 5.7 at 120 °C for both solders, respectively. Generally, the reduction of n-value has been related to the instability of the microstructure, which occurs at high deformation temperatures [21]. Since the amount of heat generated due to hot deformation is remarkably high at elevated temperatures, it cannot dissipate throughout the material owing to the higher strain rates, and could result in local static stress due to the thermal mismatch between matrix and hard ceramic nanoparticles [9,13]. However, the n-value of composite SAC 305 solder is higher than that of plain SAC305 specimen at all temperature ranges, since the β-Sn grains are finer in case of the former than in the latter. These results are quite consistent with those reported for some composite SAC solders [4,21]. The activation energy Q can be expressed as the slope of ln ($\dot{\varepsilon}$) against $1/T$ (Fig. 10). The result for activation energy indicated that the Q values are considerably changed with ZnO addition. The average Q values of 65.6 and103.7 kJ mol^{-1} were obtained for plain SAC 305 and composite SAC 305 solders, respectively. It is highly possible that the change in activation energy with different initial microstructure for both alloys is well consistent with the change in mechanical strength of two solders. Composite SAC(305)–0.7%ZnO solder featured small β-Sn grain size with high grain boundary area and fine IMC particles, which dramatically increased the hardening degree and prevented further slip of dislocations in the β-Sn matrix. As a result, deformation became difficult and activation energy increased for SAC(305)–0.7%ZnO solder. The fact that the ZnO nanoparticles may accumulate inside the β-Sn matrix and grain boundary area is a direct approval that the ZnO nanoparticles are effective as nucleation sites for IMCs crystallization and β-Sn grains. It may also restrain the dislocation density or grain boundary sliding mechanism. However, the experimental n and Q values have been frequently used to identify the mechanism controlling the deformation process. For plain SAC 305 alloy, the obtained n and Q values are close to n and Q values reported for dislocation pipe diffusion of β-Sn and SAC (4–7.5 and 40–65 kJ/mol), and are almost half those of lattice diffusion (approximately100 kJ/mol) [6]. For the composite SAC 305 solder, the Q value of 103.7 kJ/mol is in good agreement with the 100 kJ/mol obtained for lattice diffusion of β-Sn and SAC solders [22]. The observed change in the mechanism controlling the deformation process for two alloys can be ascribed to their respective microstructures shown in Fig. 3. Notably, adding the reinforcement ZnO particles could restrict the grain growth of the developed composite SAC(305)–0.7%ZnO solder. According to the classical heterogeneous nucleation theory, the existence of ZnO nanopaticles will reduce the thermodynamic barrier of β-Sn nucleation in order to increase the nucleation rate of IMC particles and refine β-Sn grain size. As a result, it can improve the mechanical properties of the composite solder.

4. Conclusions

The effect of ZnO nanoparticles' addition on the microstructure and thermal and mechanical properties of Sn–3.0Ag–0.5Cu lead-free solder has been studied in this work. The main conclusions obtained are as follows:

(1) Microstructure investigations revealed that the average size of β-Sn as well as the IMC particles were drastically reduced with the addition of nano-sized ZnO particles into the SAC(305) solder. The composite SAC(305)–0.7%ZnO solder appeared with a finer microstructure due to the high nucleation density and surface-free energy on the β-Sn grain surface promoted by ZnO nanoparticles.
(2) Significant improvement in 0.2%YS and UTS is realized with the addition of ZnO nanoparticles into the SAC(305) solder, whereas the ductility was stunted at all temperature ranges and strain rates investigated. The improved strength of SAC (305)–0.7%ZnO composite solder is due to the homogeneous distribution of ZnO nanoparticles and the refined β-Sn grain size as well as IMC particles, which can act as reinforcement phases.
(3) Addition of ZnO nanoparticles into the SAC(305) solder maintained the melting temperature of composite SAC(305)–0.7% ZnO solder at the SAC(305) level. However, the undercooling phenomenon during cooling was slightly increased although the pasty range was decreased.
(4) According to the obtained n and Q values, it is proposed that the dislocation pipe diffusion is the dominant deformation mechanism for plain SAC 305 alloy, while the lattice diffusion mechanism is dominant for the composite SAC 305 solder at all temperature ranges investigated. Notably, the difference in activation energy values was attributed to the difference in the initial microstructures of both alloys due to ZnO nanoparticles' addition.

References

[1] L.M. Yin, X.P. Zhang, C. Lu, J. Electron. Mater. 38 (10) (2009) 2179–2183.
[2] L. Ma, Y. Zuo, S. Liu, Fu Guo, X. Wang, J. Appl. Phys. 113 (2013) (044904–044904-7).
[3] M. Sona, K.N. Prabhu, J. Mater. Sci.: Mater. Electron. 24 (2013) 3149–3169.
[4] A.A. El-Daly, A. Fawzy, S.F. Mansour, M.J. Younis, Mater. Sci. Eng. A 578 (2013) 62–71.
[5] Y. Tang, G.Y. Li, Y.C., J. Alloys Compd. 554 (2013) 195–203.
[6] A.A. El-Daly, A.E. Hammad, G.S. Al-Ganainy, M. Ragab, Mater. Sci. Eng. A 608 (2014) 130–138.

[7] D.A. Shnawah, M.F.M. Sabri, L.A. Badruddin, S. Said, Microelectron. Int. 29 (2012) 47–57.
[8] A.A. El-Daly, A.M. El-Taher, T.R. Dalloul, Mater. Des. 55 (2014) 309–318.
[9] A.A. El-Daly, A. Fawzy, S.F. Mansour, M.J. Younis, J. Mater. Sci.: Mater. Electron. 24 (2013) 2976–2988.
[10] J. Shen, Y.C. Liu, D.J. Wang, H.X. Gao, J. Mater. Sci. Technol. 22 (2006) 529–532.
[11] L.C. Tsao, S.Y. Chang, Mater. Des. 31 (2010) 990–993.
[12] L.C. Tsao, S.Y. Chang, C.I. Lee, W.H. Sun, C.H. Huang, Mater. Des. 31 (2010) 4831–4835.
[13] T.H. Chuang, M.W. Wu, S.Y. Chang, S.F. Ping, L.C. Tsao, J. Mater. Sci.: Mater. Electron. 22 (2011) 1021–1027.
[14] A. Fawzy, S.A. Fayek, M. Sobhy, E. Nassr, M.M. Mousa, G. Saad, J. Mater. Sci.: Mater. Electron. 24 (2013) 3210–3218.
[15] A.A. El-Daly, A.E. Hammad, G.S. Al-Ganainy, A.A. Ibrahiem, Mater. Des. 56 (2014) 594–603.
[16] N. Hamada, T. Uesugi, Y. Takigawa, K. Higashi, J. Alloys Compd. 527 (2012) 226–232.
[17] A.A. El-Daly, A.M. El-Taher, T.R. Dalloul, J. Alloys Compd. 587 (2014) 32–39.
[18] L.C. Tsao, Mater. Sci. Eng. A 529 (2011) 41–48.
[19] X. Wang, Y.C. Liu, C. Wei, H.X. Gao, P. Jiang, L.M. Yu, J. Alloys Compd. 480 (2009) 662–665.
[20] A.A. El-Daly, A.E. Hammad, Mater. Des. 40 (2012) 292–298.
[21] A.A. El-Daly, A. Fawzy, S.F. Mansour, M.J. Younis, Mater. Des. 55 (2014) 837–845.
[22] A.R. Geranmayeh, G. Nayyeri, R. Mahmudi, Mater. Sci. Eng. A 547 (2012) 110–119.

View publication stats